Acoustic propagation in realistic 3D nonlinear internal waves

Alec J. Duncan (1), Kenji Shimizu (2), Iain M. Parnum (1), Rod MacLeod (3), Steve Buchan (4)

(1) Centre for Marine Science and Technology, Curtin University, GPO Box U 1987, Perth, 6845, Western Australia
(2) Civil Engineering, Kobe University, 1-1 Rokkodaicho, Nada-ku, Kobe 657-8501, Japan
(3) Maritime Division, Defence Science and Technology Group, HMAS Stirling, Rockingham, Western Australia
(4) RPS MetOcean, 31 Bishop Street, Jolimont, Western Australia

ABSTRACT

Nonlinear internal waves are a feature of many continental margins, particularly those with large tidal ranges such as Australia's Northwest Shelf. This paper extends previous work on the effects of idealised nonlinear internal waves on acoustic propagation at mid-frequency sonar frequencies to the case of a realistic, fully three-dimensional, time evolving internal wave field. The internal wave field was modelled using MITgcm, which is a state of the art, three-dimensional, non-hydrostatic hydrodynamic model. Time evolving, three-dimensional sound velocity fields were calculated from the MITgcm temperature and salinity outputs and used as input to the Bellhop3D acoustic propagation model, which was used to calculate the variations in transmission loss that occurred as a nonlinear internal wave train crossed the acoustic transmission path. Results were broadly consistent with those obtained previously using the idealised internal wave train but predicted somewhat smaller changes in transmission loss between horizontally focussed and defocussed conditions of up to 18 dB compared to changes of up to 30 dB obtained with the idealised internal waves. Analysis of more events is required in order to test the robustness of this result.

1 INTRODUCTION

This study follows on from work reported in Parnum et. al. (2017), and Duncan et al. (2018), that investigated the effect of nonlinear internal waves typical of Australia's Northwest Shelf on acoustic propagation at a frequency of 7 kHz. The 2017 study concentrated on sound propagation perpendicular to the internal wave crests; whereas, the 2018 report presented the results of three dimensional propagation modelling for a direction parallel to the internal wave crests, where horizontal refraction effects play a dominant role. However, the Parnum et. al. (2017) and Duncan et al. (2018) studies used a simplistic model of nonlinear internal waves to calculate the time-varying three-dimensional sound velocity field that was used for acoustic propagation modelling. The simplified internal wave model used by Parnum et. al. (2017) and Duncan et al. (2018) was non-dispersive, with infinitely long, straight, wave crests propagating in constant depth water. Consequently, Duncan et al. (2018) recommended replacing the simplistic internal wave model with a more realistic model that captured the fully three-dimensional shape of these waves. As a result, Defence Science and Technology Group commissioned RPS Australia West Pty. Ltd. to carry out three-dimensional nonlinear internal wave modelling for an area on Australia's Northwest Shelf where measured data are available and where these types of waves are known to occur. RPS carried out the modelling using the MIT General Circulation Model (MITgcm) nonlinear internal wave model (Marshall et al., 1997). MITgcm is a numerical model designed for study of the atmosphere, ocean, and climate. Its non-hydrostatic formulation enables it to simulate fluid phenomena over a wide range of scales; its adjoint capability enables it to be applied to parameter and state estimation problems (MITgcm, 2019). By employing fluid isomorphisms, one hydrodynamic kernel can be used to simulate flow in both the atmosphere and ocean. For theoretical details about MITgcm see Marshall et al. (1997). MITgcm has been shown to a useful tool to model oceanographic internal waves (Shimizu and Nakayama, 2017). The results produced by the MITgcm model for this study were consistent with measured data (Shimizu, 2019).

As in Duncan et al. (2018), this study utilised the Bellhop3D beam tracing model written by Michael B Porter. Bellhop 3D is a generalisation of the well-known Bellhop model (also written by Dr Porter), to include both vertical and horizontal refraction effects and also to include out of plane seabed reflections. See Jensen et. al. (2011) for the theoretical basis for both these models and Porter (2016) for details of Bellhop3D. Being a beam tracing model, Bellhop3D was well-suited to the frequency of interest for this study (7 kHz); however, like any acoustic

propagation model it is important that its input parameters are carefully chosen in order to obtain accurate results. Parameter selection was investigated in detail in Duncan et al. (2018), and the results of that study were used to inform the choice of parameters for this project.

2 METHODS

2.1 Oceanograhic modelling

This study is based on an 18 km x 18 km area off north western Australia (Figure 1). The primary source of bathymetry was the 2009 version of Geosciences Australia bathymetry (Whiteway, 2009). This bathymetry was manually adjusted in the 70 to 300-m depth range to match model bathymetry to the measured water depths at the ARC and IMOS moorings. An additional data set was necessary for the revised model domain because Geosciences Australia bathymetry does not cover north of 8ºS. In the revised grid, Geosciences Australia bathymetry was smoothly merged with the global SRTM15+ bathymetry (Becker et al., 2009) over the Indian Ocean. A subset of the MITgcm output grid was used from a 2-hour interval during which it was traversed by a packet of nonlinear internal waves. Two sets of data were analysed, one sampled every 20 s for the full 2-hour interval, and one sampled every 4 s for a 10 minute period in the middle of the 2-hour interval.

2.2 Sound field data

The MITgcm model outputs data in NETcdf format files, with each file providing data for all required time slices for a sub-grid known as a tile. For this study, 70 tiles were required to cover the 18 km x 18 km study area. Three output files for each tile were used: one providing static grid coordinate data, one providing dynamic potential temperature data, and the third providing dynamic salinity data. The MITgcm model output was on a rotated spherical grid, with the chosen parameters corresponding to spacings of 27.79 m and 55.59 m in X and Y respectively. The vertical grid spacing was 5 m for depths from 2.5 m to 97.5 m after which it increased towards a maximum spacing of 11.4 m just above the deepest grid point (138.4 m). Note that, as a result of the rotation of the grid, the X and Y axes are not in the cardinal directions (see Figure 1).

To create sound field data compatible with the Bellhop3D model, the data outputted from the MITgcm model required the following steps: 1) the tiled data were reassembled into a single spatial grid; 2) the temperature data was converted from potential temperature to absolute temperature; and 3) the sound speed was calculcated from the temperature, salinity and depth/pressue data. The sound speed data were then saved as a series of MATLAB data files, with each file providing the three dimensional sound speed field over the entire grid for one time. The Matlab functions used to make the temperature and sound speed calculations were from the CSIRO "Seawater" library (Morgan, 1993) which is based on Fofonoff et. al. (1983).

2.3 Acoustic propagation modelling

The parameters that were used for the Bellhop3D modelling are listed in Table 1. These parameters were based on the results of sensitivity tests described in Duncan and Parnum (2018), and were the same as those used in that study except where the different geometry dictates otherwise. The 2018 work assumed a flat seabed, however the MITgcm output included the bathymetry grid used when calculating the internal wave field, so this was exported in the format required by Bellhop3D and included in the acoustic modelling.

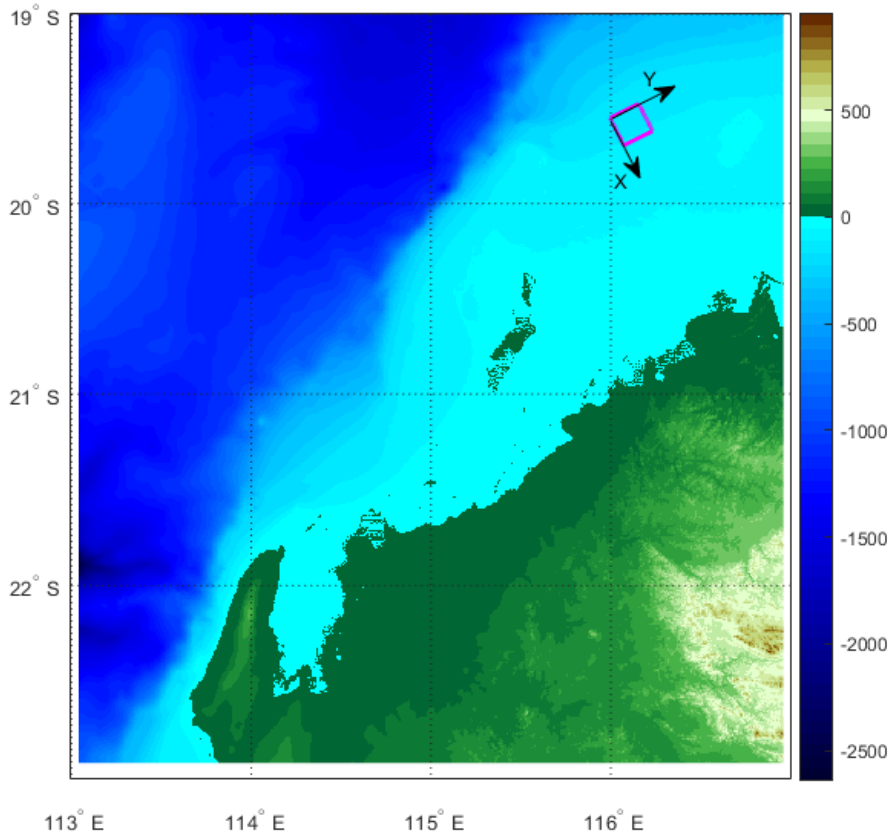

Figure 1: Map showing the boundary of the 18 km x 18 km grid (magenta square) off north western Australia and the directions of the X and Y axes.

Table 1: Parameters used in the Bellhop3D modelling.

Parameter	Value
Frequency	7 kHz
Source position (Z positive down)	X = 13500 m, Y = 3600 m, Z = 10 m
Water depth range	107.2 m to 139.5 m
Maximum receiver range	15 km
Beam type	B (Gaussian beams)
Run type for transmission loss calculations	I (Incoherent transmission loss)
Run mode	Full 3D
Calculation box size (X, Y, Z)	(16000 m, 14000 m , 160 m)
Seabed compressional sound speed (m/s)	1770
Seabed density	1894 $kg.m^{-3}$
Seabed compressional wave attenuation	0.8 dB/wavelength
Receiver bearings from source	116° (direction of positive X axis)
Receiver depths	35 m, 95 m, 95 m
Receiver ranges	1000:1000:15000
Elevation beam fan for transmission loss calculations	-40°:0.2°:40°
Bearing beam fan relative to receiver azimuth for transmission loss calculations	-5°:0.05°:5°

3 RESULTS

Figure 2 shows the modelled transmission loss (TL) vs time for receiver ranges of 5 km, 10 km and 15 km, and at depths of 35 m (Figure 2 - top) and 95 m (Figure 2 - bottom). These plots may be placed in context by referring to Figure 3 which shows sound speed fields and ray traces for two times of particular interest indicated as vertical dashed lines on the transmission loss time series plots in Figure 2. Prior to the arrival of the internal wave train, the sound speed field is quite uniform in the horizontal plane in the vicinity of the acoustic propagation path, and the rays are essentially straight (not shown). The fluctuations in the TL increase slightly from about 3000 s, but only significantly at a range of 15 km (Figure 2). The sound speed maximum corresponding to the first wave in the nonlinear internal wave-train occurs at the receivers at 3600 s. The crest (maximum sound velocity) of the first wave in the internal wave-train lies along the propagation path and refracts sound away from the 10 km and 15 km receivers (Figure 3 (a) and (b)), resulting in an increase in TL (Figure 2). This is the "defocused" condition. The situation is reversed about ten minutes later at 4160 s, at which time a sound speed minimum lies along the transmission path, forming a horizontal duct that focuses the sound and sharply reduces the TL at the 10 km and 15 km receivers (Figure 3 (c) and (d)).

The effects of the internal waves on TL increase with range along the acoustic propagation path, but in this scenario the receiver depth had little effect (Figure 2). At a range of 5 km, the TL fluctuations are only a few dB (Figure 2). This is partly because of the short range, and partly because the sound speed changes due to the internal waves are relatively small over the first third of the transmission path. However, at 10km the effects of the internal waves on TL are much larger, resulting in periods of about 10 minutes during which the transmission loss is increased by about 3 dB compared to its average value prior to the arrival of the wave train, separated by much shorter periods during which the transmission loss is up to 10 dB lower than its quiescent value (Figure 2). When the receiver is at 15 km, the periods of increased and decreased transmission loss are more equal, both being a little less than 10 minutes, and result in fluctuations in TL from about 8 dB below to 10 dB above the quiescent value (Figure 2). At both 10 km and 15 km range the fluctuations in the transmission loss reduce in amplitude as the later (Figure 2), lower amplitude waves in the internal wave train cross the transmission path.

The results shown in Figure 2 and Figure 3 used sound field data sampled every 20 s. Comparison between the transmission loss for the 4 s and 20 s sample interval data found that at 5 km range the relatively slow variations in TL appeared to be adequately tracked by the 20 s sample interval data. The situation was similar for much of the time at 10 km range (Figure 4 - top), although it is notable that the peak at 4140 s appears to be undersampled by the 20 s data. Consquenetly, the height of the peak TL at 10 km was being underestimated by as much as 3 dB at the 95 m deep receiver. At a range of 15 km, there were seemingly random TL fluctuations of as much as 1 dB between consecutive 4 s interval samples, particularly during periods when the TL is changing rapidly, however, the 20 s sample interval seems adequate to capture the main features of the TL variations (Figure 4 - bottom).

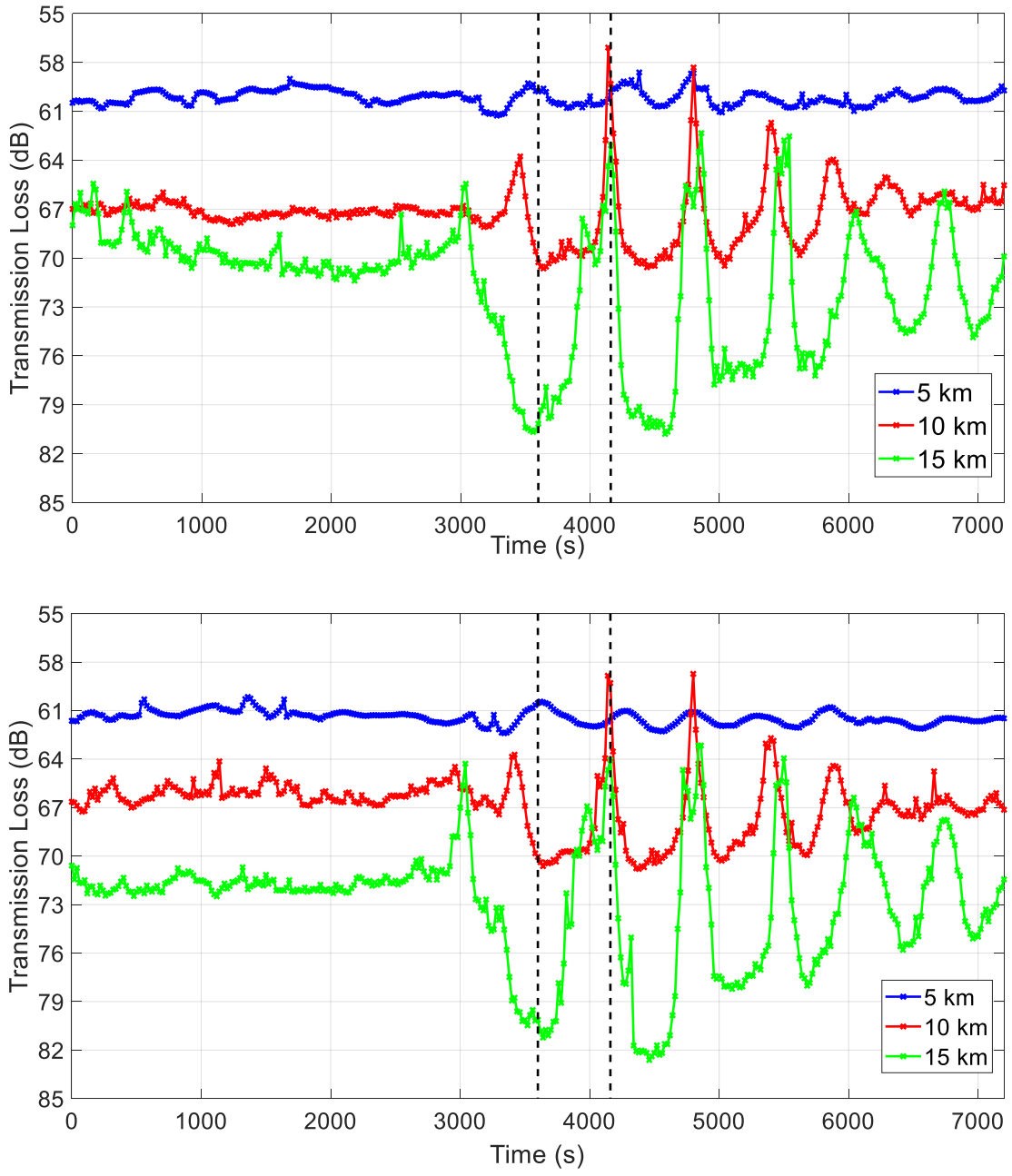

Figure 2: Modelled transmission loss vs. time to a receiver at ranges of 5, 10 and 15 km and depths of: 35 m (top) and 95 m (bottom). Vertical dash-dot lines at 3600 and 4160 s correspond to the ray trace and sound speed plots shown in Figure 3.

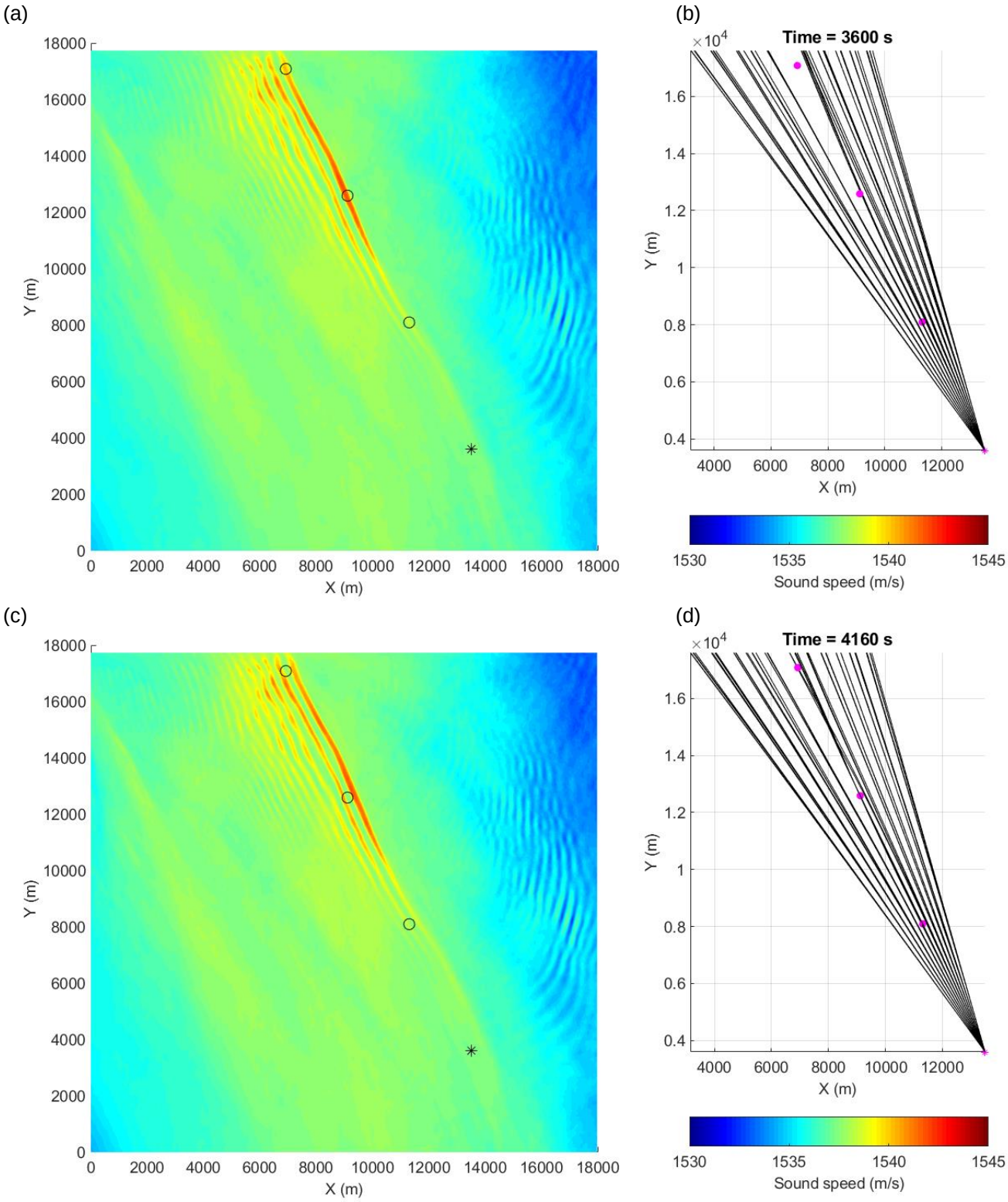

Figure 3: Horizontal slice through the sound speed field at a depth of 60 m (left column) and ray traces (right column). Asterisks and circles show the source and receiver positions respectively. For times of: 3600 s (a) and (b); and 4160 s (c) and (d).

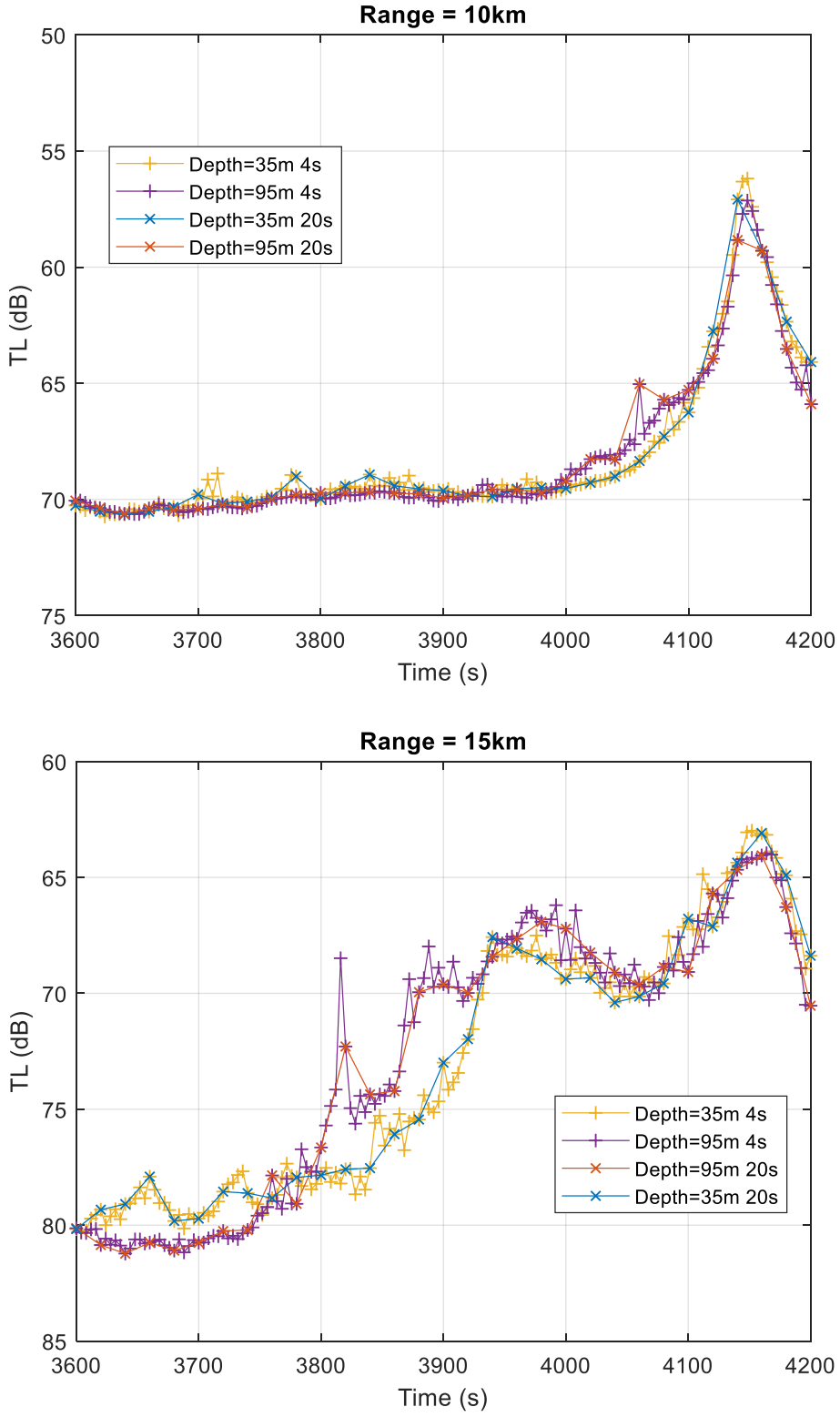

Figure 4: Comparison between modelled transmisison loss vs time curves obtained using sound velocity fields sampled at 4 s and 20 s intervals for a range of 10 km (top) and 15 km (bottom).

4 CONCLUSIONS

The results presented here are qualitatively very similar to those obtained previously using the idealised internal wave model (Duncan and Parnum 2018), with the TL at 15 km exhibiting similar rapid changes in TL between focussed and defocussed states during the passage of a nonlinear internal wave-train. In both cases, the oscillation period is about 15 minutes. Quantitatively, the current work predicts smaller changes in TL than those seen in the previous study, with a difference in TL of about 18 dB between focussed and unfocussed states compared to up to 30 dB seen with the idealised model. However, not too much should be read into this preliminary result as only one transmission path and one internal wave event have been modelled so far. Future work will therefore involve modelling other transmission paths and other internal wave events to further understand the magnitude of fluctuations of TL in internal waves fields found in NW Australia.

ACKNOWLEDGEMENTS

The authors would like to thank the Defence Science and Technology Group for funding this study.

REFERENCES

Becker, J. J., D. T. Sandwell, W. H. F. Smith, J. Braud, B. Binder, Jl Depner, D. Fabre et al. "Global bathymetry and elevation data at 30 arc seconds resolution: SRTM30_PLUS." *Marine Geodesy* 32, no. 4 (2009): 355-371.

Duncan, Alec J., Iain M. Parnum, and Rod MacLeod. "The effect of internal waves on sound propagation parallel to the internal wave crests." In *Proceedings of ACOUSTICS*, vol. 7, no. 9. 2018.

Fofonoff, Nicholas Paul, and R. C. Millard Jr. "Algorithms for the computation of fundamental properties of seawater." (1983). Unesco Tech. Pap. in Mar. Sci., No. 44, 53 pp

Marshall, John, Alistair Adcroft, Chris Hill, Lev Perelman, and Curt Heisey. "A finite-volume, incompressible Navier Stokes model for studies of the ocean on parallel computers." *Journal of Geophysical Research: Oceans* 102, no. C3 (1997): 5753-5766.

MITgcm. [MIT General Circulation Model] http://mitgcm.org/ (Accessed: 23rd July 2019)

Mohsen, B., Katsnelson, B.G., Lynch, J.F., Pereselkov, S. and W. L. Siegmann. "Measurement and modeling of three-dimensional sound intensity variations due to shallow-water internal waves." *The Journal of the Acoustical Society of America* 117, no. 2 (2005): 613-625.

Parnum, I. M., McLeod, R., Duncan, A. J., Gavrilov, A. N., “The effect of internal waves on underwater sound propagation”. *Proceedings, Acoustics 2017, Perth*, 19-22 November, 2017

Shimizu, K., "3d internal solitary wave modelling for acoustic propagation studies", RPS Report 100-CN-REP-1831 REVA, 9th April 2019.

Shimizu, Kenji, and Keisuke Nakayama. "Effects of topography and Earth's rotation on the oblique interaction of internal solitary-like waves in the Andaman Sea." *Journal of Geophysical Research: Oceans* 122, no. 9 (2017): 7449-7465

Whiteway, T. G. "Australian bathymetry and topography grid." *Geoscience Australia, Canberra* (2009).